Article

Not peer-reviewed version

Indirect Voltammetry Detection of Non-Electroactive Neurotransmitters using Glassy Carbon Microelectrodes: The Case of Glutamate

Sandra Lara Galindo , Surabhi Nimbalkar , Alexis Oyawale , James Bunnell , Omar Nunez Cuacuas , Rhea Montgomery-Welsh , Amish Rohatgi , Brinda Kodira Cariappa , Abhivyakti Gautam , Kevin Peguero-Garcia , Juyeon Lee , Stephanie Ingemann Bisgaard , Carter Faucher , Stephan Sylvest Keller , Sam Kassegne *

Posted Date: 9 May 2024

doi: 10.20944/preprints202405.0577.v1

Keywords: glassy carbon; voltammetry; glutamate; neurotransmitters; FSCV; Microelectrodes

Article

Indirect Voltammetry Detection of Non-Electroactive Neurotransmitters using Glassy Carbon Microelectrodes: The Case of Glutamate

Sandra Lara Galindo [1,2], Surabhi Nimbalkar [1,2], Alexis Oyawale [1,2], James Bunnell [1,2], Omar Nunez Cuacuas [1,2], Rhea Montgomery-Welsh [1,2], Amish Rohatgi [1,2], Brinda Kodira Cariappa [1,2] Abhivyakti Gautam [1,2], Kevin Peguero-Garcia [1,2], Juyeon Lee [1,2], Stephanie Ingemann Bisgaard [3], Carter Faucher [1,2], Stephan Sylvest Keller [3] and Sam Kassegne [1,2,*]

[1] NanoFAB.SDSU Research Lab., Department of Mechanical Engineering, College of Engineering, San Diego State University, 5500 Campanile Drive, San Diego, CA 92182-1323, USA
[2] NSF-ERC Center for Neurotechnology (CNT)
[3] National Centre for Nano Fabrication and Characterization, DTU Nanolab, Technical University of Denmark, Ørsteds Plads, Building 347, 2800 Kongens Lyngby, Denmark
* Correspondence: kassegne@sdsu.edu; Tel: +(760)-402-7162

Abstract: Glassy carbon (GC) microelectrodes have been successfully used for detection of electroactive neurotransmitters such as *dopamine* and *serotonin* through voltammetry. However, non-electroactive neurotransmitters such as *glutamate, lactate*, and *gamma-aminobutyric acid* (*GABA*) are inherently unsuitable for detection through voltammetry techniques without functionalizing the surface of the microelectrodes. To that end, we present here the immobilization of *L-glutamate oxidase* (*GluOx*) enzyme on the surface of GC microelectrodes to enable catalysis of chemical reaction between *L-glutamate*, oxygen, and water to produce H_2O_2, an electroactive byproduct that is readily detectable through voltammetry. This immobilization of *GluOx* on the surface of bare GC microelectrodes and the subsequent catalytic reduction of H_2O_2 through fast scan cyclic voltammetry (FSCV) helped demonstrate indirect *in vitro* detection of *glutamate*, a non-electroactive molecule, at concentrations as low as *10 nM*. The functionalized microelectrodes formed part of 4-channel arrays of microelectrodes (30 µm x 60 µm) on a 1.6 cm long neural probe supported on a flexible polymer, with potential for *in vivo* applications. The type and strength of the bond between the GC microelectrode surface and its functional groups on one hand, and *glutamate* and the immobilized functionalization matrix on the other hand, were investigated through molecular dynamics (MD) modeling and Fourier Transform Infrared Spectroscopy (FTIR). Both MD modeling and FTIR demonstrated the presence of several covalent bonds in the form of *C-O (carbon-oxygen polar covalent bond), C=O (carbonyl), C-H (alkenyl), N-H (hydrogen bond), C-N (carbon-nitrogen single bond), and C≡N* (triple carbon nitrogen bond). Further, penetration tests on agarose hydrogel model confirmed that the probes are mechanically robust with their penetrating forces being much lower than the fracture force of the probe material.

Keywords: glassy carbon; voltammetry; glutamate; neurotransmitters; FSCV; Microelectrodes

1. Introduction

Neurotransmitters play a pivotal role in a large variety of neurophysiological functions [1-4]. For example, *dopamine* (DA) is involved in several neurophysiological processes such as motor control, reward, motivation and cognitive function [5-8] whereas *serotonin* (*5-Hydroxytryptamine* (*5-HT*)) plays a significant role in several neural signal processes such as memory, long-term potentiation as well as cardiovascular and gastrointestinal functions [9-12]. The disruption of the secretion and uptake of *DA* and *5-HT* at synapses is considered as causative factor towards several psychiatric and neurological disorders [12-15]. Further, while *5-HT* is a major target for pharmacological treatment, its involvements in mood disorders as well as neuroplasticity is still of

 doi:10.20944/preprints202405.0577.v1

significant research and clinical interest [16]. *Glutamate* and *lactate*, two closely related neurotransmitters, are involved in the metabolic pathways of the central nervous system (CNS), with *glutamate* being the most extensive free-standing amino acid in the brain with its increased presence identified as a potential cause for significant neuronal cell damage or epileptic seizure [17-22]. Given their significant roles, the understanding of electrochemical neural signaling enabled by neurotransmitters could, therefore, help develop a more complete picture of brain functions and better insight into some key neurological disorders [22-26]. Further, integration of neurochemical sensing with electrophysiological recording and stimulation is of fundamental importance in elucidating the relationship between electrical and electrochemical signaling and their role in the pathogenesis of neurological disorders [27-29]. This increased understanding could also inform the design of novel closed-loop treatment platforms enabled by neurochemical feedback [30-32]. Therefore, there is a continuing research need for developing new electrode technology for detection of these neurotransmitters *in vivo*.

From a detection point of view, neurotransmitters can be broadly classified into two general groups, i.e., electroactive and non-electroactive. For example, *dopamine, serotonin, and adenosine* are electroactive species that can electrochemically oxidize forming *quinone* groups [33-35]. Techniques such as fast scan cyclic voltammetry (FSCV) can then be used for direct detection of such electroactive species through their respective signature redox peaks. On the other hand, neurotransmitters such as *glutamate*, *lactate*, *acetylcholine*, and *gamma-aminobutyric acid (GABA)* are non-electroactive and are, therefore, inherently unsuitable for direct detection through voltammetry techniques. For this and several other reasons such as no requirement for specialized equipment and post-processing of data, most works reported in the literature in the detection of such non-electroactive neurotransmitters had used amperometric techniques [36-37]. However, the major drawback of amperometric technique is its non-selectivity, which – in the context of simultaneous detection of multiple neurotransmitters – makes it impractical for such needs. This has given rise to the exploration of FSCV for detection of *glutamate* along with other neurotransmitters such as *dopamine*. In one such reported work, GlutOx-chitosan hydrogels were electrodeposited on carbon-fiber microelectrodes (CFM) where enzymatic generation of electroactive hydrogen peroxide helped detect *glutamate* [38]. However, carbon-fiber microelectrodes have their own shortcomings such as lack of mechanical sturdiness and inconsistent composition and surface adsorption properties that have in turn limited their repeatability and reliability [39].

To address these gaps, recent works have introduced a lithographically patternable array of carbon-based microelectrodes that have shown promises in neurotransmitter detections. Among these, glassy carbon (GC) has emerged as a compelling material of choice for microelectrodes used in the detection of electroactive neurotransmitters, such as *DA* and *5-HT* at concentrations as low as 10 nM [40-46]. Further, due to its surface that is rich with electrochemically active functional groups, good adsorption characteristics, and its antifouling properties, GC has been demonstrated to be useful for not only electrophysiological recording and stimulation, but also for multi-site simultaneous detection of the electroactive neurotransmitters, *DA* and *5-HT* in a stable and repeatable manner [45-46]. However, for the indirect detection of non-electroactive neurotransmitters such as *glutamate*, *lactate*, and the like, surface functionalization of the microelectrodes is required. One such possibility is the immobilization of *glutamate oxidase* (*GluOx*) enzyme on the surface of microelectrodes to enable catalysis of the chemical reaction between *L-glutamate*, oxygen, and water to produce the electroactive byproduct *hydrogen peroxide* that is detectable through voltammetry (*L-glutamate + oxygen + water → oxoglutarate + ammonia + hydrogen peroxide*). In lieu of *GluOx*, *glutamate dehydrogenase* could also be used for detection of *glutamate* [47-49]. In this study, we extend the application of GC to detection of non-electroactive neurotransmitters and present the immobilization of *GluOx* on lithographically patterned GC microelectrodes for establishing the indirect electrochemical *in vitro* detection of *glutamate*. The same platform could be used for the detection of other neurotransmitters through the appropriate surface functionalization.

 doi:10.20944/preprints202405.0577.v1

2. Materials and Methods

2.1. Microfabrication of Microelectrodes

A 1.6 cm long penetrating neural probe with four GC microelectrodes of 30 µm x 60 µm size was microfabricated. As described elsewhere, the microfabrication process for the probe shown in Figure 1a involved spin-coating of SU-8 negative photoresist (Microchem, MA) on a silicon wafer (with 0.5 µm thick oxide layer) at 1200 rpm for 55 s and soft-baking at 65°C for 10 min and 95°C for 20 min followed by UV exposure at ~400 mJ/cm^2 [50]. This was followed by a post-exposure bake at 65°C for 1 min and 95°C for 5 min, development of SU-8 for 3–5 min and curing at 150°C for 30 min. Pyrolysis was done at 1000°C in an inert N_2 environment following protocols described elsewhere [50-52]. Subsequently, 5 µm layer of photo-patternable polyimide (HD 4100) (HD Microsystems, DE, USA) was spin-coated on top of the GC microelectrodes at 2500 rpm for 45 s, soft baked at 90°C for 3 min and at 120°C for 3 min, then cooled down to room temperature, and patterned through UV exposure at ~400 mJ/cm^2. Then, the polyimide layer was partially cured at 300°C for 60 min under N_2 environment. Following, Pt metal traces with Ti adhesion layer were patterned using a metal lift-off process. For electrical insulation, an additional 6 µm of polyimide HD 4100 was spin-coated (300 rpm), patterned (400 mJ/cm^2), and cured (350°C for 90 min) under N_2 environment. An additional 30 µm thick layer of polyimide (Durimide 7520, Fuji Film, Japan) was spin-coated (800 rpm, 45 s) and then patterned (400 mJ/cm^2) on top of the insulation layer to reinforce the penetrating portion of the device (Figure 1b). Once the probes were released from the carrier substrate using a BHF bath, the GC microelectrodes were plasma etched (120W for 45 s) and then functionalized through drop-casting of a thin coat of an enzyme mix.

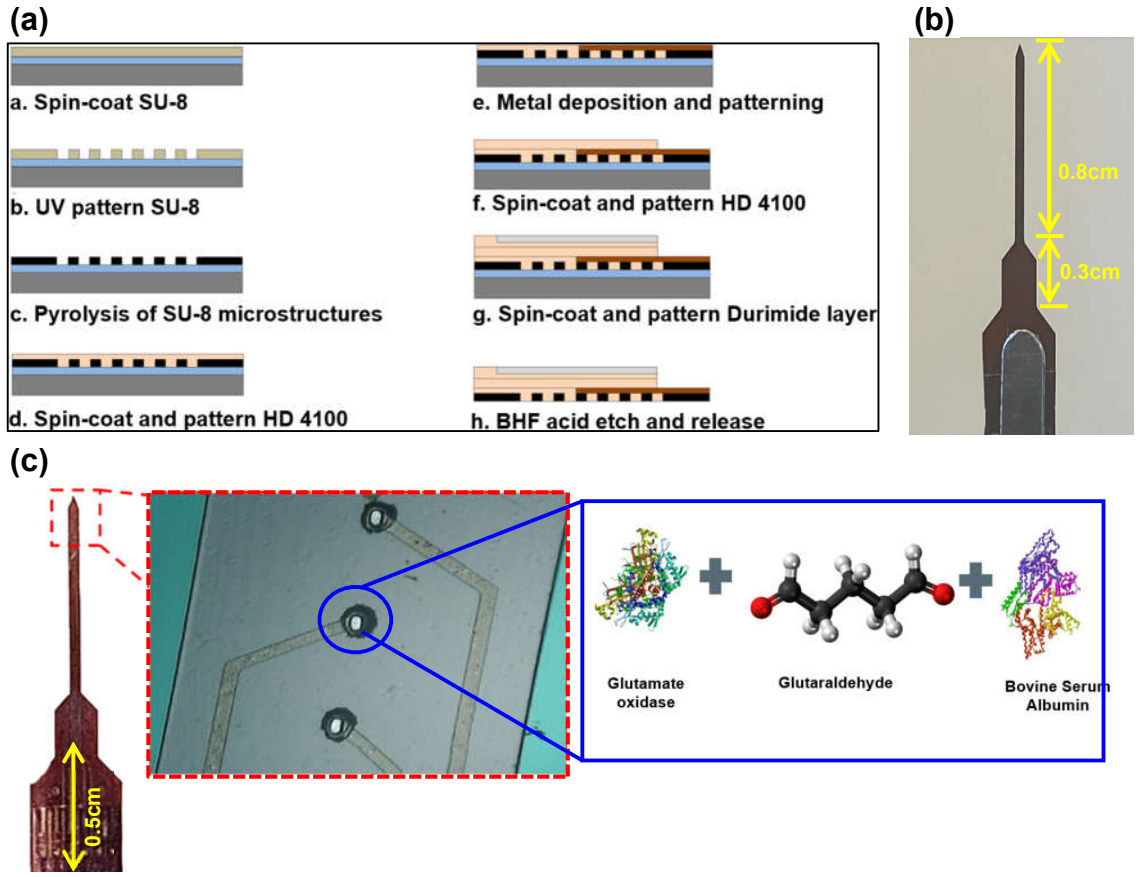

Figure 1. (a) microfabrication steps for *4-channel* penetrating neural probes (1.6 cm long) mounted on polymeric substrate (b) fabricated probe for neurotransmitter detection application (c) GC microelectrodes of 30 µm x 60 µm size and 140 µm spacing coated with the *GluOx*, *glutaraldehyde*, and *BSA* mixture.

 doi:10.20944/preprints202405.0577.v1

2.2. Functionalization of Microelectrodes

As shown in Figures 1c, the surface functionalization process consisted of preparing an enzyme immobilization matrix made of *glutamate oxidase* (*GluOx*), a catalytic enzyme, *glutaraldehyde (*a reagent from the aldehyde family that allows a rapid ionic immobilization of the enzyme on the GC microelectrode surface), and *bovine serum albumin* (*BSA*) which provides stability to the enzyme and the reagent mixture. *L-glutamic acid* (≥99%), *L-glutamate oxidase* (from S*treptomyces sp.),* and *bovine serum* albumin (≥ 96%) were purchased from Sigma Aldrich (St. Louis, MO). In addition, *glutaraldehyde* (25% solution distillation purified) was purchased from Electron Microscopy Sciences (PA, USA). Before mixing, *GluOx*, *glutaraldehyde,* and *BSA* were brought to room temperature. Then, the *GluOx* enzyme was dissolved in 1 µL of DI water. Separately, 0.01g of *BSA* was placed in a microcentrifuge tube and 985 µL of DI water added to it. The mix was then vortexed at low rpm. Subsequently, 5 µL of *glutaraldehyde* was added. This mixture of *BSA*/*glutaraldehyde* was then transferred into a 500 µL microcentrifuge tube, 1 µL of *GluOx* was added to it and it was vortexed again at slow rpm. This was followed by dry storage of the immobilization matrix at room temperature to ensure a successful crosslinking between the enzyme, *glutaraldehyde* and *BSA*. Finally, 10 µL of the immobilization matrix was then extracted and pipetted for drop-casting of a thin coat over the surface of the GC microelectrodes.

2.3. Mechanical Characterization

The mechanical stability of the probes and their penetration ability were tested using a TA.XT plusC Texture Analyzer (TA) (Stable Micro Systems Products). To determine an appropriate agarose gel concentration that models the modulus of brain tissue, a compression calibration test was first carried out as explained in the accompanying supplementary document (Section S1) [53-56]. Once the relevant concentration of agarose gel was determined, penetration tests of the *in vitro* model medium were carried out using the GC probes presented in Figure 1. For this, a holder for the GC probe was designed, 3D printed and mounted on the probe of the TA (Figure 2). The agarose gel block shown in Figure 2 had a length of 30 mm, width of 30 mm, thickness of 10 mm, and area of 900 mm^2. The same speed of loading of 2 mm/s was used for the penetration test as well, with a 0.5 kg weight load cell.

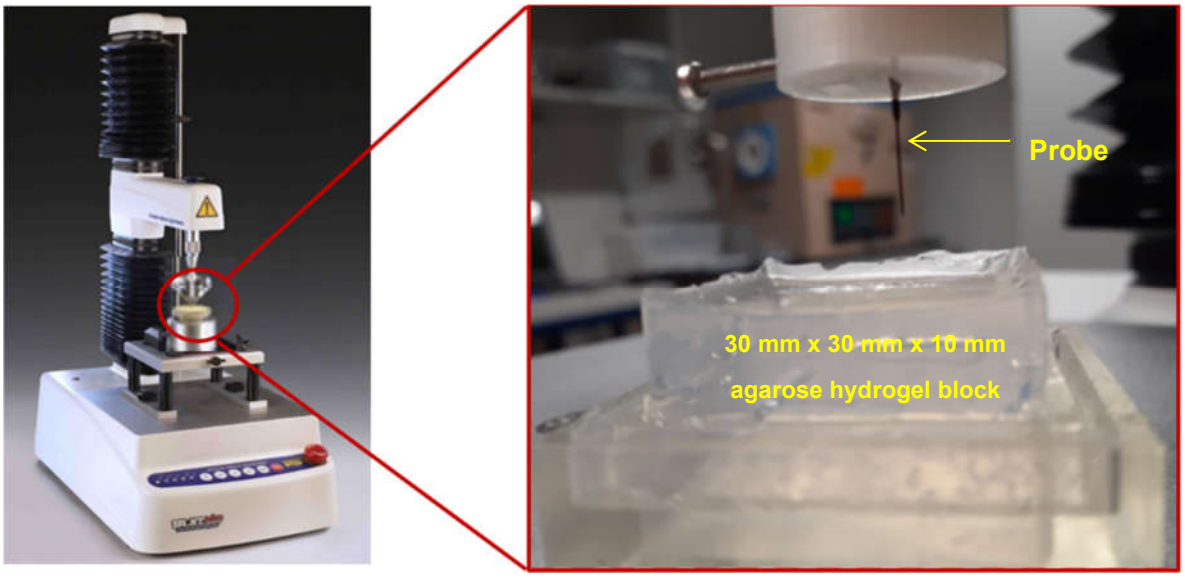

Figure 2. TA.XT plusC Texture Analyzer holding a probe for penetration tests.

2.4. Molecular Dynamics (MD) Modeling

To understand the interaction between *glutamate* and the immobilized enzyme mix with the surface of GC microelectrodes and investigate if covalent bonds were formed, a chemical simulation

 doi:10.20944/preprints202405.0577.v1

was performed using molecular dynamics (MD) modeling software. We used ReaxFF software from SCM-ReaxFF, a tool for modeling chemical reactions with a reactive force field [57]. Briefly, in this reactive force field formulation of ReaxFF, a pre-determined potential energy function allows for the calculation of the force experienced by any atom, given the positions of all its surrounding atoms at a given time step. The forces acting on each atom at each time step are computed using molecular mechanics force fields. The position and velocity of each atom and energy contributions to the potential are then updated using Newton's Equations of Motion. The total force consists of the energy associated with forming bonds between atoms, the valence angle strain and torsional angle strain, and electrostatic and dispersive contributions between all atoms. The starting model of the molecular structure of GC was the nanostructure that was reported in our recent work consisting of a flat graphitic domain with graphene-like *6-membered* carbon rings and a cage-like component [58]. For simplicity, the simulation cell used here (*25 Å x 25 Å x 25 Å*) with a density of 1.19 g/mL models only the flat component consisting of 144 graphene-like *6-membered* carbon rings as shown in Figure 3. Four functional groups (*carbonyl*, *carboxyl*, *hydroxyl*, and *epoxy*) were considered attached to this carbon molecule. The *5-* and *7-membered* carbon rings that form the periphery of the cagey component along with *6-membered* carbon rings are expected to have similar chemical interactions and are not included in the model to save computational expenses.

With regard to modeling *GluOx* which is a relatively large protein structure, the significantly high computational resources required could be a limiting factor. However, since all proteins and amino acids contain both *C-* and *N*-terminal domains, the amino acid *glutamate* can be taken as a smaller representation of the large molecule of *GluOx*, thereby achieving a more efficient way of predicting chemical interactions between the key amino acid components and the carbon surface. This is further supported by the fact that *glutamate* is one of seven amino acids present in the active site of *GluOx*, suggesting that it plays an essential role in the production of H_2O_2. A full list of key amino acids that are present in the active site, along with their functional groups, are listed in Table S1 for completeness. With this reasoning, *glutamate* ($C_5H_9NO_4$) molecule was added to the simulation cell. Two temperature cases (27°C and 37°C) and two voltage bias cases (0 V and 0.4 V) were considered. All models were analyzed using a temperature damping constant of *100 fs* and a pressure damping constant of 500 fs with constant volume and temperature conditions through the constant temperature and volume (NVT) Berendsen thermostat [59-60].

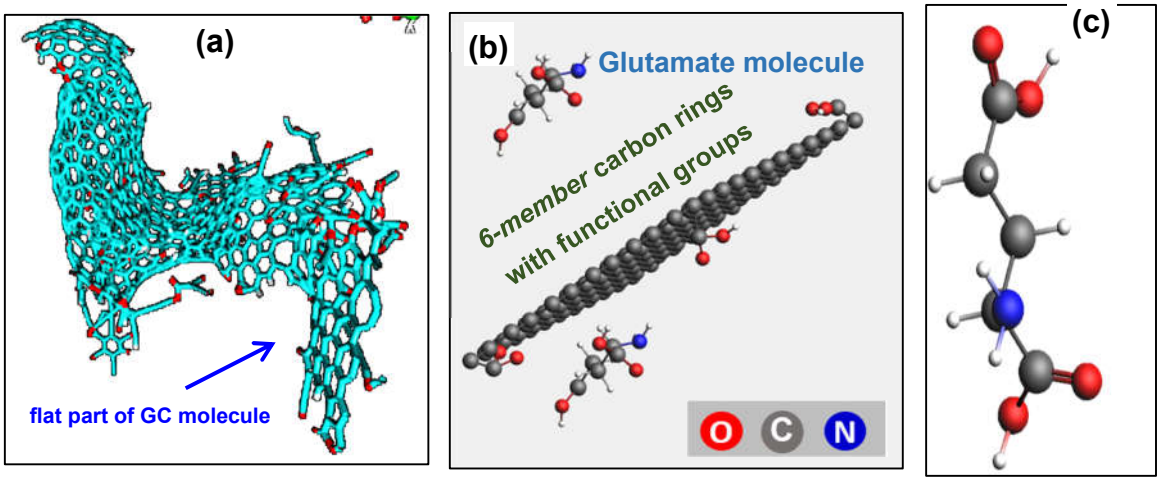

Figure 3. (a) GC molecule [58] (b) MD model consisting of only *6-membered* carbon rings with functional groups (carbonyl, carboxyl, hydroxyl, and epoxy) and *glutamate* molecules in a simulation cell of 25 Å x 25 Å x 25 Å (c) single *glutamate* ($C_5H_9NO_4$) molecule which is considered here to represent an active site of *GluOx*.

 doi:10.20944/preprints202405.0577.v1

2.5. FTIR Spectroscopy

To determine the presence of functional groups and, by correlation, the strength of the bond between the GC microelectrode surface and the immobilized functionalization mix, FTIR-ATR spectroscopy was carried out using a Nicolet iS50 FTIR Spectrometer equipped with a Smart iTR diamond ATR cell (Thermo Scientific, Court Vernon Hills, IL, USA). Three types of samples were analyzed: a bare GC microelectrode that was used as control, a plasma-etched GC microelectrode (120W for 45 s) with a coating of *GluOx* mixture containing *glutaraldehyde* and *BSA*, and a GC microelectrode with a *GluOx* mixture without *glutaraldehyde* and *BSA*. Each sample was washed with methanol, dried, and placed on the diamond cell, followed by recordings of 128 spectral scans that were subsequently compiled from 4 diagonal areas of the microelectrodes.

2.6. Voltammetry

Indirect detection of *glutamate* through direct electrochemical detection of the conversion product H_2O_2 was performed with a WaveNeuro Potentiostat System (Pine Research, NC). The surface functionalized GC microelectrode was used as the working electrode with a standard Ag/AgCl reference electrode. The electrolyte solution was *phosphate-buffered saline* (PBS) (0.01 M, pH 7.4; Sigma Aldrich, USA). A waveform consisting of triangle scan at scan rate of *400 V/s* from *−0.5 V to +1.3 V* with a holding potential of *-0.5 V* with respect to Ag/AgCl reference electrode was used. The duration of each scan was *9 ms* and the frequency was *10 Hz*. The same voltage waveform was applied to microelectrodes at *60 Hz* for 1 hour prior to the start of each experiment for preconditioning. Known concentrations of *glutamate* (10 nM – 1.6 µM) were then infused over 5 sec while changes in current were recorded for 30 s. For a control experiment, a separate probe with no surface functionalization was subjected to the same waveform.

3. Results and Discussion

3.1. Mechanical Characterization

Figure 4 shows the force-displacement plots for the penetration force test with the neural probe for agarose hydrogel of 0.6% concentration, which was found to be a good model for brain tissue (Section S2). The first clearly identifiable peak shown in Figure 4 corresponds to the first section of the neural probe penetrating the surface of the gel. The penetration force is then the first maximum of the force-displacement curve. The force needed for penetration of the 0.6% agarose hydrogel simulating the brain tissue was 0.0035 ± 0.00015 N ($n = 5$) while for the 1.5% agarose hydrogel, the penetration force was 0.0051 ± 0.00028 N ($n = 4$).

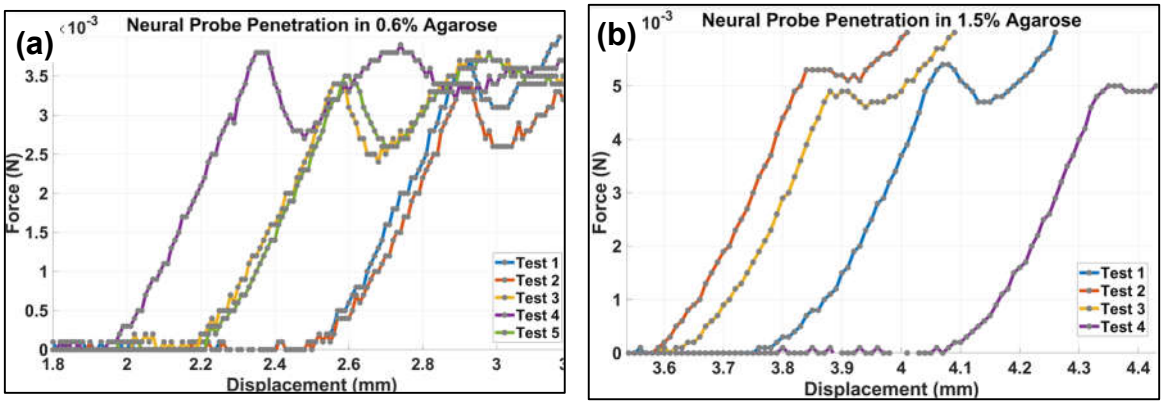

Figure 4. Penetration force measurements for (a) 0.6% and (b) 1.5% agarose gel concentrations.

3.2. Molecular Dynamics Modeling

We explored the interaction of the functional groups (*COOH, CO, OH, and O*) on the carbon microelectrode material with *glutamate* and the immobilized enzyme mix. For this, we considered the

 doi:10.20944/preprints202405.0577.v1

effect of electrical bias (0V, 0.4 V), temperature (25°C and 37°C), type of functional groups, number of molecules of *glutamate*, and the lattice of the *6-member* carbon ring group on this interaction. Several potential interactions with functional groups to produce covalent bonds were explored. As shown in Figure 5a, the *carboxyl (COOH)* functional group was observed to interact with *glutamate* at a temperature of 25°C with no electrical bias with the *glutamate* molecule forming a carbon-oxygen (*C-O*) covalent bond with the functionalized GC microelectrode surface. This interaction occurred due to the donation of electrons by *glutamate*. The epoxide group was observed to facilitate the formation of a strong carbon-nitrogen (*C-N*) covalent bond between nitrogen molecule from *glutamate* and the carbon molecule of the microelectrode (Figure 5b). However, at this temperature and 0 voltage bias, no interactions were observed for *carbonyl (CO)* and *hydroxyl (OH)* functional groups. Considering a slightly higher temperature of 37°C, the carbonyl functional group (*CO*) results in a *C=O* covalent bond (Figure 5c).

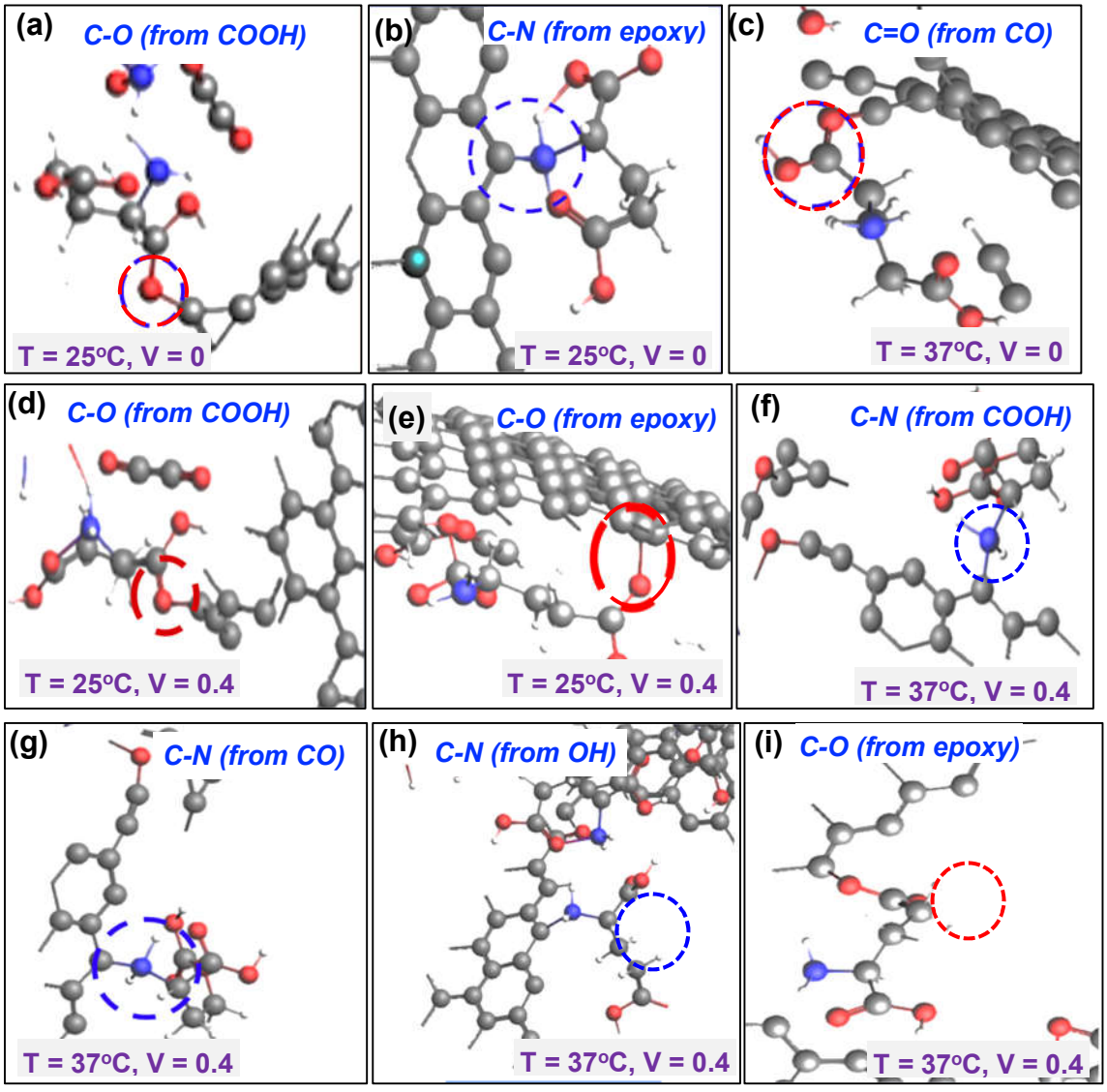

Figure 5. (a) *C-O* bond due to *COOH* group at 25°C and no bias (b) *C-O* bond due to epoxy group at 25°C and no bias (c) *C=O* bond due to carbonyl group at 37°C and no bias (d) *C-O* bond due to *COOH* group at 0.4 V and 25°C (e) *C-O* bond due to epoxy at 0.4 V and 25°C (f) *C-N* bond due to *COOH* group at 0.4 V and 37°C (g) *C-N* bond due to *CO* group at 0.4 V and 37°C (h) *C-N* bond due to OH group at 0.4 V and 37°C (i) *C-O* bond due to epoxy at 0.4 V and 37°C.

In the next set of simulations, the effect of electrical bias was explored under temperatures of 27°C and 37°C. In the case of temperature of 25°C, similar outcomes as for the 0 V bias case were

 doi:10.20944/preprints202405.0577.v1

observed (Figures 5d and 5e). However, at the temperature of 37°C, all the four functional groups were observed to enable formation of a covalent bond between *glutamate* and the carbon microelectrode surface. In the case of carboxyl group, increasing the temperature to 37°C combined with electrical bias at 0.4 V resulted in a carbon-nitrogen (*C-N*) bond (Figure 5f). Similarly, for carbonyl group, increasing the temperature to 37°C led to carbon-nitrogen (*C-N*) bond as shown in Figure 5g, demonstrating the effect of elevated temperature for forming bonds. For hydroxyl group, a carbon-nitrogen (*C-N*) bond was observed, while in the case of epoxide group, an immediate attachment of *glutamate* through a carbon-oxygen (C-O) bond was observed. A summary of the interactions is presented in Table 1.

Table 1. Summary of the interaction of the four functional groups on the carbon electrode surface with enzyme mix and glutamate. Simulation cell of *25 Å x 25 Å x 25 Å* was considered with sphere radius of 2 Å.

Voltage/Bias (V)	Temp. (°C)	Functional Group	Outcome	Figure
0	25	COOH (carboxyl)	*C-O bond*	Figure 5a
		CO (carbonyl)	No bond	
		OH (hydroxyl)	No bond	
		O (epoxy)	*C-N bond*	Figure 5b
	37	COOH (carboxyl)	No bond	
		CO (carbonyl)	*C=O*	Figure 5c
		OH (hydroxyl)	No bond	
		O (epoxy)	No bond	
0.4	25	COOH (carboxyl)	*C-O bond*	Figure 5d
		CO (carbonyl)	No bond	
		OH (hydroxyl)	No bond	
		O (epoxy)	*C-O bond*	Figure 5e
	37	COOH (carboxyl)	*C-N bond*	Figure 5f
		CO (carbonyl)	*C-N bond*	Figure 5g
		OH (hydroxyl)	*C-N bond*	Figure 5h
		O (epoxy)	*C-O bond*	Figure 5i

3.3. FTIR Characterization

For the bare GC control specimen (inset in Figure 6a), three clear and distinct peaks that ranged between *1435.67 cm^{-1} - 755.53 cm^{-1}* were detected, representing *C-O* stretch with a single bond [61]. The second sample had its bare GC surface plasma-etched at *120 W* for *45 seconds* before coating it with *glutamate oxidase* mixture. Figure 6a summarizes several peaks for the *glutamate oxidase* sample on top of GC: the first peak at *3488.55 cm^{-1}* corresponds to the amine stretch (*N-H*) that potentially originated from unreacted amino groups in *glutamate oxidase* and *L-glutamate* [62], while the peak at *3071.12 cm^{-1}* corresponds to alkenyl (*C-H)* stretch and its neighbor peak of *3000 cm^{-1}* corresponds to unsaturated alkene (*C=C*) compounds. Carboxylic acid (*C=O*) peaks are represented by stretch in the region of *1775.28 cm^{-1} - 719.52 cm^{-1}* while (*C-H*) bending vibration with single or multiple absorption bands is represented by *719.52 cm^{-1}* [63]. For the third sample that was coated with *glutamate oxidase*, more peaks were detected as shown in Figure 6b where the characteristic absorption ranged between *2136.93 cm^{-1} - 534.48 cm^{-1}*. The highest fingerprint was *2136.9 cm^{-1}* that is a triple bond between carbon and nitrogen stretch *(C≡N)*, and the second peak was *1753.04 cm^{-1}* which corresponds to an aldehyde *C=O* stretch; this one, in particular, is derived from the *glutaraldehyde* present on the surface of the microelectrode from the enzyme mixture [64].

 doi:10.20944/preprints202405.0577.v1

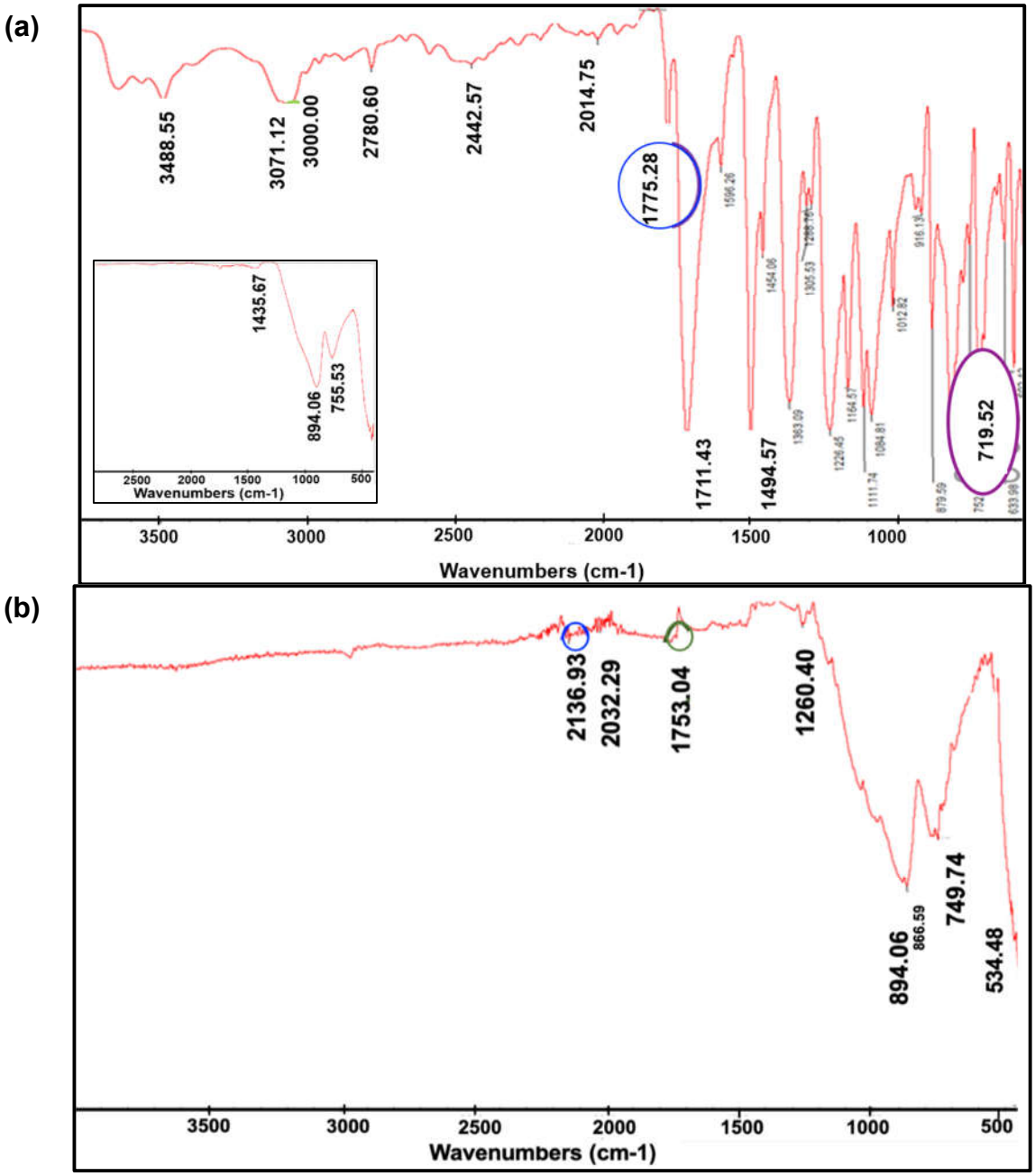

Figure 6. (**a**) FTIR spectra for plasma-etched GC electrode coated with *glutamate enzyme* (*GluOx* mixture containing *glutaraldehyde* and *BSA*) (**b**) spectra for *glutamate oxidase* analyzed on top of GC electrode surface. Inset shows the FTIR for bare GC.

3.4. In Vitro Glutamate Detection through Voltammetry

As described earlier, due to the non-electroactive nature of *glutamate*, background-subtracted FSCV for *glutamate* was performed indirectly through the immobilization of *glutamate oxidase* (*GluOx*) enzyme on the surface of GC microelectrodes. The *GluOx* enabled catalysis of chemical reaction between *L-glutamate*, oxygen, and water to produce an electroactive byproduct (H_2O_2) that is readily detectable through voltammetry. Since typical FSCV runs result in accelerated oxidation and reduction of electroactive and non-electroactive species on the electrode surface and hence form an electrical double layer, the background currents (BC) were subtracted before the peaks could be identified [63]. As a control, the first set of experiments involved injecting solution of H_2O_2 on bare GC microelectrode at varying concentrations over a period of 25 minutes (Table S2). Figure 7a shows the resulting redox peaks in a background-subtracted FSCV for H_2O_2 with oxidation occurring at 1.2V

 doi:10.20944/preprints202405.0577.v1

and reduction at -0.2V [66]. As the second set of control experiment, FSCV was carried out on bare GC electrodes where *glutamate* of varying concentration was injected. However, there was no redox peaks observed for this control experiment. On the other hand, for the actual experiment, another probe was used where *glutamate* of varying concentration (10 nM – 1.6 µM) was injected to PBS solution. This was done over a period of 30 minutes as shown in Table S2, with sufficient time provided in-between each step to allow for stabilization of FSCV data collection. Figure 7b shows the resulting background-subtracted FSCV plots indicating that the GC microelectrode was able to detect the *glutamate conversion* byproduct H_2O_2 obtained at a *glutamate* concentration as low as *10 nM* with *an* oxidation peak at 1.2 V and reduction peak at -0.2 V. False-color plot of Figure 8a shows the transient oxidation and reduction of 200 nM of H_2O_2 injected to PBS solution (control). The false-color plot for injection of 10 nM of *glutamate* to PBS PBS solution is shown in Figure 8b.

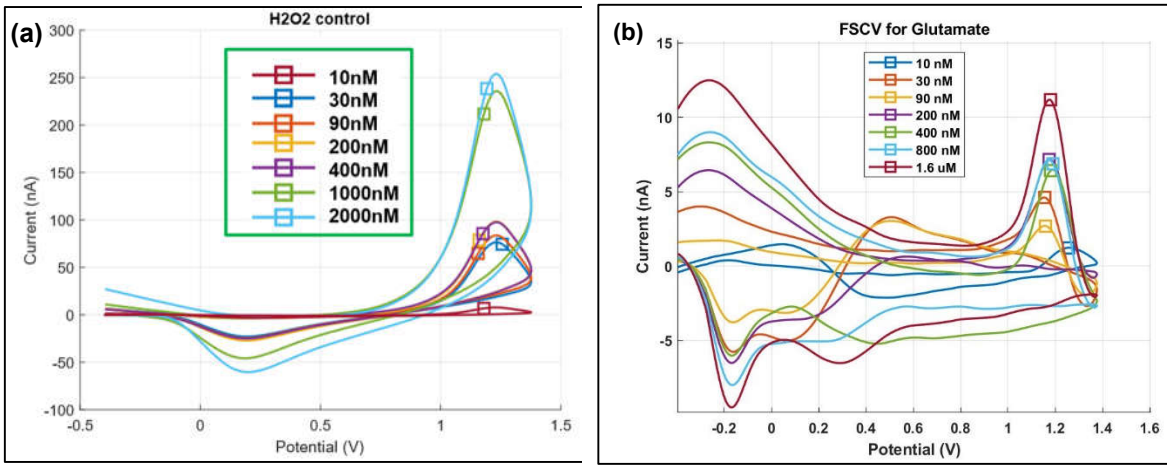

Figure 7. (a) Redox peaks in FSCV during detection of H_2O_2 of varying concentration used for control experiment (10 nM - 2 µM). Redox peaks in FSCV during indirect *glutamate* detection at several concentrations (10 nM - 1.6 µM).

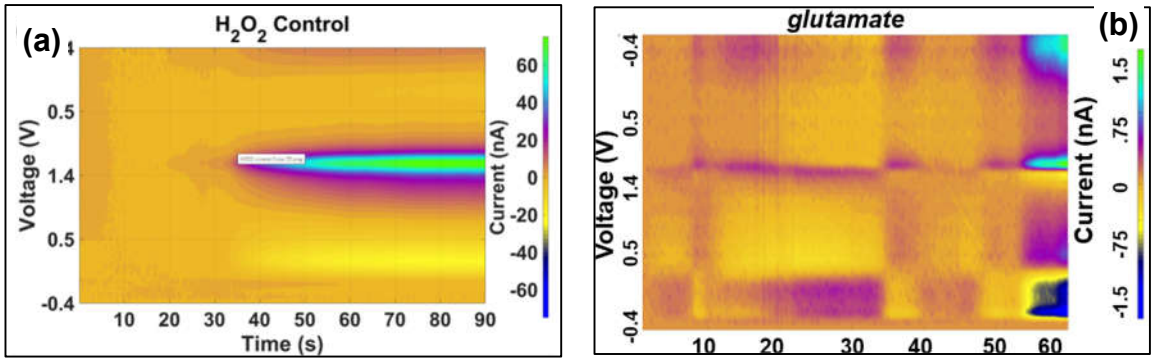

(**a**) (**b**)

Figure 8. (a) 2D false-color plot corresponding to addition of *200 nM* concentration of H_2O_2 (b) 2D false-color plot corresponding to addition of *10 nM* concentration of *glutamate* to PBS solution.

4. Discussions and Conclusion

While GC has been demonstrated to be effective in detecting electroactive neurotransmitters such as *dopamine* and *serotonin* at concentrations as low as 10 nm, its potential use for non-electroactive ones like *glutamate* has been so far unexplored. Against a background of a long-term research interest in the simultaneous detection of multiple neurotransmitters using GC voltammetry electrodes located on the same probe, the extension of this capability of GC to such detection of non-electroactive analytes like *glutamate* carries potential for significant contribution in the broader research discipline of neurochemistry. In this regard, the first obstacle that had to be addressed in extending its capability to glutamate was the integrity of the needed surface functionalization. Two

 doi:10.20944/preprints202405.0577.v1

approaches were sought to demonstrate formation of covalent bond between the carbon surface and the enzymes used for surface functionalization, i.e., FTIR and reactive molecular dynamics (MD) modeling. FTIR confirmed the existence of *C-O* stretch with a single bond, an aldehyde/carboxylic/carbonyl *C=O* stretch, alkenyl *C-H* bending, a triple bond between nitrogen and carbon stretch *(C≡N)*, an amine stretch (*N-H*) that potentially originated from unreacted amino groups in *glutamate oxidase* and *L-glutamate*. On the other hand, MD modeling predicted *C-O and C=O* bonds arising due to *carboxyl (COOH*) and *epoxy (O)* functional groups at 25°C and 37°C and no bias conditions. However, in the presence of a nominal voltage bias of 0.4 V and temperature of 37°C, *carboxyl, carbonyl (CO),* and *hydroxyl (OH)* groups were observed to interact with *glutamate* forming a *C-N* bond. The absence of amine stretch (*N-H*) in the MD simulation could be explained by the absence of unreacted amino groups in the model.

In general, these results obtained through reactive MD modeling are consistent with what was recently reported in a simulation work regarding the binding properties of pristine graphene and graphene derivatives with *glutamate* where the bond formations were driven mainly by the same four functional groups, i.e., *COOH*, *carbonyl*, *hydroxyl*, and *epoxy* [65]. Further, simulation based on molecular docking mechanisms between the functional groups and carbon (in the form of graphene) also demonstrated that the *COOH* functional group presented the highest stability among the four groups considered. The observation that all functional groups located on the surface of the electrode formed some sort of covalent bond with *glutamate* at a physiologically relevant temperature of 37°C with a nominal voltage bias is very encouraging and builds a case for the effectiveness of GC as a *glutamate* sensing electrode material. The presence of these bonds also points to a potential durability of this surface functionalization. In addition, for fast detection of analytes with low-detection limits, diffusion and then subsequent adsorption of the analytes on the surface of the electrode are important and critical components. While prior work on the diffusion of glutamate towards carbon surfaces is missing in the literature, the demonstration of adsorption through bond formation here is an important outcome that further supports the effectiveness of GC for sensing *glutamate* at low detection limits.

With the presence of strong covalent bonds between surface of GC electrode and the functionalization enzyme established, the next task was demonstrating the validity and effectiveness of indirect voltammetric detection of *glutamate* through its by-product of H_2O_2. The evidence presented in this research indicates strong correlations between H_2O_2 and *glutamate*, enabling detection of 10 nM concentration of *glutamate*, an important milestone. In general, therefore, the data presented here from *the in vitro* detection of *glutamate* are promising, with the modified GC electrodes capable of detecting a wide range of concentrations of the byproduct of enzymatic *glutamate* conversion. Testing penetration of the probe in agarose gel based *in vitro* brain models confirmed that the probe used in this experiment is appropriate for brain penetration. Validation of the *in vitro* data presented here through *in vivo* testing, demonstration of detection of other non-electroactive neurotransmitters such as *lactate*, and – more importantly - the simultaneous detection of electroactive and non-electroactive neurotransmitters on the same probe will form a natural extension of this current work.

Author Contributions: S.L.G fabricated the devices, implemented the microfabrication process, analyzed the results and wrote the materials and methods and results sections of the paper; S.N helped set up the molecular dynamics simulations; A.O helped in microfabrication; J.B helped with plots and analysis; O.N.C helped with SEM imaging; R.M.W. helped set up the molecular dynamics simulations; A.R helped in microelectrode characterization; B.K.C and A.G helped in microfabrication; K.P.G helped with FTIR; J.L helped with MATLAB plots; S.I.B designed and carried out the mechanical characterizations; C.F helped with chemistry of *glutamate oxidase* and *glutamate* as they relate to MD modeling, S.S.K reviewed the manuscript; and S.K. formulated the concept, supervised the project, structured the outline of the paper, edited the manuscript, and wrote the introduction, discussion and conclusion section of the paper.

Acknowledgments: This material is based on research work supported by the Center for Neurotechnology (CNT), a National Science Foundation Engineering Research Center (EEC-1028725). S.I.B. and S.S.K acknowledge funding from the Independent Research Fund Denmark (Grant no. 8022-00215B).

Conflicts of Interest: The authors declare no competing financial interests.

References

1. Si, Bo, and Edward Song. 2018. "*Recent Advances in the Detection of Neurotransmitters*." *Chemosensors* 6 (1): 1–24. https://doi.org/10.3390/chemosensors6010001.
2. Puskarjov, Martin, Patricia Seja, Sarah E. Heron, Tristiana C. Williams, Faraz Ahmad, Xenia Iona, Karen L. Oliver, et al. 2014. "*A Variant of KCC2 from Patients with Febrile Seizures Impairs Neuronal Cl- Extrusion and Dendritic Spine Formation*." EMBO Reports 15 (6): 723–29. doi.org/10.1002/embr.201438749.
3. Lotharius, Julie, and Patrik Brundin. 2002. "*Pathogenesis of Parkinson's Disease: Dopamine, Vesicles and α-Synuclein*." Nature Reviews Neuroscience 3 (12): 932–42. https://doi.org/10.1038/nrn983.
4. Gründer, G., and P. Cumming. 2016. "*Computational Neuroanatomy of Schizophrenia*." *The Neurobiology of Schizophrenia* 1: 263–82. https://doi.org/10.1016/B978-0-12-801829-3.00023-9.
5. Wise, Roy A. 2004. "*Dopamine, Learning and Motivation*." Nature Reviews Neuroscience 5 (6): 483–94. https://doi.org/10.1038/nrn1406.
6. Haber, Suzanne N., and Brian Knutson. 2010. "*The Reward Circuit: Linking Primate Anatomy and Human Imaging*." *Neuropsychopharmacology* 35 (1): 4–26. https://doi.org/10.1038/npp.2009.129.
7. Ryczko D, Dubuc R. 2017. "*Dopamine and the Brainstem Locomotor Networks: From Lamprey to Human*," Frontiers in Neuroscience 11: 295
8. Felger, Jennifer C., and Michael T. Treadway. 2017. "*Inflammation Effects on Motivation and Motor Activity: Role of Dopamine*" Neuropsychopharmacology 42 (1): 216–41. https://doi.org/10.1038/npp.2016.143.
9. Pithadia, Anand. 2009. "*5-Hydroxytryptamine Receptor Subtypes and Their Modulators with Therapeutic Potentials*." Journal of Clinical Medicine Research 1 (2): 72–80. https://doi.org/10.4021/jocmr2009.05.1237.
10. Maffei, Massimo E. 2021. "*5-Hydroxytryptophan (5-HTP): Natural Occurrence, Analysis, Biosynthesis, Biotechnology, Physiology and Toxicology*." International Journal of Molecular Sciences 22 (1): 1–25. https://doi.org/10.3390/ijms22010181.
11. Franco, Rafael, Rafael Rivas-Santisteban, Jaume Lillo, Jordi Camps, Gemma Navarro, and Irene Reyes-Resina. 2021. "*5-Hydroxytryptamine, Glutamate, and ATP: Much More Than Neurotransmitters.*" Frontiers in Cell and Developmental Biology 9 (April): 1–8. https://doi.org/10.3389/fcell.2021.667815.
12. Gründer, G., & Cumming, P. (2016). "*The Dopamine Hypothesis of Schizophrenia: Current Status*," In T. Abel & T. Nickl-Jockschat (Eds.), The Neurobiology of Schizophrenia (pp. 109–124). Elsevier Academic Press. https://doi.org/10.1016/B978-0-12-801829-3.00015-X.
13. Fakhoury, Marc. 2016. "*Revisiting the Serotonin Hypothesis: Implications for Major Depressive Disorders.*" *Molecular Neurobiology* 53 (5): 2778–86. https://doi.org/10.1007/s12035-015-9152-z.
14. Schloss, Patrick, and D. Clive Williams. 1998. "*The Serotonin Transporter: A Primary Target for Antidepressant Drugs.*" Journal of Psychopharmacology 12 (2): 115–21. doi.org/10.1177/026988119801200201.
15. Yohn, Christine N., Mark M. Gergues, and Benjamin Adam Samuels. 2017. "*The Role of 5-HT Receptors in Depression", Molecular Brain* 10 (1): 1–12. doi.org/10.1186/s13041-017-0306-y.
16. Celada, Pau, M. Victoria Puig, and Francesc Artigas. 2013. "*Serotonin Modulation of Cortical Neurons and Networks*." *Frontiers in Integrative Neuroscience* 7 (APR 2013): 1–20. https://doi.org/10.3389/fnint.2013.00025.
17. Zhou, Y., & Danbolt, N. C. (2014). "*Glutamate as a Neurotransmitter in the Healthy Brain*," Journal of Neural Transmission, 121(8), 799–817. https://doi.org/10.1007/s00702-014-1180-8
18. Ramadan, Saadallah, Alexander Lin, and Peter Stanwell. 2013. "*Glutamate and Glutamine: A Review of in Vivo MRS in the Human Brain.*" NMR in Biomedicine 26 (12): 1630–46. https://doi.org/10.1002/nbm.3045.
19. Barker-Haliski, Melissa, and H. Steve White. 2015. "*Glutamatergic Mechanisms Associated with Seizures and Epilepsy*." Cold Spring Harbor Perspectives in Medicine 5 (8): 1–15.
20. Statstrom, C.E, and L. Carmant. 2016. "*Seizures and Epilepsy: An Overview*." Epilepsy: The Intersection of Neurosciences, Biology, Mathematics, Engineering, and Physics, 65–77. https://doi.org/10.1201/b10866-10.
21. Beghi, Ettore. 2020. "*The Epidemiology of Epilepsy*," Neuroepidemiology 54 (2): 185–91. https://doi.org/10.1159/000503831.
22. Furness, Amanda M., Ranu Pal, Elias K. Michealis, Craig E. Lunte, and Susan M. Lunte. 2019. "*Neurochemical Investigation of Multiple Locally Induced Seizures Using Microdialysis Sampling: Epilepsy Effects on Glutamate Release.*" Brain Research 1722 (July): 146360.
23. Lee, Darrin J., Christopher S. Lozano, Robert F. Dallapiazza, and Andres M. Lozano. 2019. "*Current and Future Directions of Deep Brain Stimulation for Neurological and Psychiatric Disorders*." *Journal of Neurosurgery* 131 (2): 333–42. doi.org/10.3171/2019.4.JNS181761.
24. Moran, Sean P., James Maksymetz, and P. Jeffrey Conn. 2019. "*Targeting Muscarinic Acetylcholine Receptors for the Treatment of Psychiatric and Neurological Disorders*." *Trends in Pharmacological Sciences* 40 (12): 1006–20. https://doi.org/10.1016/j.tips.2019.10.007.
25. McCutcheon, Robert A., Tiago Reis Marques, and Oliver D. Howes. 2020. "*Schizophrenia - An Overview.*" JAMA Psychiatry 77 (2): 201–10. doi.org/10.1001/jamapsychiatry.2019.3360.
26. Poewe, Werner, Klaus Seppi, Caroline M. Tanner, Glenda M. Halliday, Patrik Brundin, Jens Volkmann, Anette Eleonore Schrag, and Anthony E. Lang. 2017. "*Parkinson Disease*." Nature Reviews Disease Primers 3: 1–21. https://doi.org/10.1038/nrdp.2017.13.

27. Kandel E.R., & Schwartz J.H., & Jessell T.M., & Siegelbaum S.A., & Hudspeth A.J., & Mack S(Eds.), (2014). *Principles of Neural Science, Fifth Edition*. McGraw Hill.
28. Ludwig, Parker E, Vamsi Reddy, and Matthew Varacallo. 2022. "*Neuroanatomy, Central Nervous System (CNS).*" In *StatPearls Publishing*. Treasure Island (FL).
29. Obien, Marie Engelene J., Kosmas Deligkaris, Torsten Bullmann, Douglas J. Bakkum, and Urs Frey. 2015. "*Revealing Neuronal Function through Microelectrode Array Recordings*." Frontiers in Neuroscience 9 (JAN): 423. doi.org/10.3389/fnins.2014.00423.
30. Pereda A. E. (2014). "*Electrical Synapses and Their Functional Interactions with Chemical Synapses*," Nature Reviews, Neuroscience,*15*(4), 250–263. https://doi.org/10.1038/nrn3708
31. Bozorgzadeh, B., Schuweiler, D. R., Bobak, M. J., Garris, P. A., & Mohseni, P. (2016). Neurochemostat: "*A Neural Interface SoC With Integrated Chemometrics for Closed-Loop Regulation of Brain Dopamine*," IEEE Transactions on Biomedical Circuits and Systems, *10*(3), 654–667. https://doi.org/10.1109/TBCAS.2015.2453791
32. Grahn, Peter J., Grant W. Mallory, Obaid U. Khurram, B. Michael Berry, Jan T. Hachmann, Allan J. Bieber, Kevin E. Bennet, *et al.* 2014. "*A Neurochemical Closed-Loop Controller for Deep Brain Stimulation: Toward Individualized Smart Neuromodulation Therapies*." Frontiers in Neuroscience 8 (8 JUN): 1–11. https://doi.org/10.3389/fnins.2014.00169.
33. Bath, B. D., D. J. Michael, B. J. Trafton, J. D. Joseph, P. L. Runnels, and R. M. Wightman. 2000. "*Subsecond Adsorption and Desorption of Dopamine at Carbon-Fiber Microelectrodes*," Analytical Chemistry 72 (24): 5994–6002. doi.org/10.1021/ac000849y.
34. Kim, Do Hyoung, Yoonbae Oh, Hojin Shin, Cheonho Park, Charles D. Blaha, Kevin E. Bennet, In Young Kim, Kendall H. Lee, and Dong Pyo Jang. 2018. "*Multi-Waveform Fast-Scan Cyclic Voltammetry Mapping of Adsorption/Desorption Kinetics of Biogenic Amines and Their Metabolites.*" Analytical Methods 10 (24): 2834–43. https://doi.org/10.1039/c8ay00352a.
35. Shadlaghani, Arash, Mahsa Farzaneh, Dacen Kinser, and Russell C. Reid. 2019. "*Direct Electrochemical Detection of Glutamate, Acetylcholine, Choline, and Adenosine Using Non-Enzymatic Electrodes*." Sensors (Switzerland) 19 (3). https://doi.org/10.3390/s19030447.
36. Okon, S. L.; Ronkainen, N. J. "*Enzyme-Based Electrochemical Glutamate Biosensors*." In Electrochemical Sensors Technology, Rahman, M. M.; Asiri, A. M., Eds.; InTech, 2017.
37. Shin, M.; Wang, Y.; Borgus, J. R.; Venton, B. J. "*Electrochemistry at the Synapse*." Annu. Rev. Anal. Chem. 2019, 12 (1), 297– 321
38. Kimble LC, Twiddy JS, Berger JM, Forderhase AG, McCarty GS, Meitzen J, Sombers LA. Simultaneous, "*Real-Time Detection of Glutamate and Dopamine in Rat Striatum Using Fast-Scan Cyclic Voltammetry*." ACS Sens. 2023 Nov 24;8(11):4091-4100. doi: 10.1021/acssensors.3c01267
39. Manciu, F.S.; Oh, Y.; Barath, A.; Rusheen, A.E.; Kouzani, A.Z.; Hodges, D.; Guerrero, J.; Tomshine, J.; Lee, K.H.; Bennet, K.E. "*Analysis of Carbon-Based Microelectrodes for Neurochemical Sensing.*" Materials 2019, 12, 3186. https://doi.org/10.3390/ma12193186
40. Swinya, Dalia L., Daniel Martín-Yerga, Marc Walker, and Patrick R. Unwin. 2022. "*Surface Nanostructure Effects on Dopamine Adsorption and Electrochemistry on Glassy Carbon Electrodes*." Journal of Physical Chemistry C 126 (31): 13399–408. https://doi.org/10.1021/acs.jpcc.2c02801.
41. Khoshnevisan, Kamyar, Elham Honarvarfard, Farzad Torabi, Hassan Maleki, Hadi Baharifar, Farnoush Faridbod, Bagher Larijani, and Mohammad Reza Khorramizadeh. 2020. "*Electrochemical Detection of Serotonin: A New Approach*." Clinica Chimica Acta 501 (November 2019): 112–19.
42. Mendoza, A, Asrat, T., Liu, F., Wonnenberg, P., and Zestos, A.G., 2020. "*Carbon Nanotube Yarn Microelectrodes Promote High Temporal Measurements of Serotonin Using Fast Scan Cyclic Voltammetry*." *Sensors (Switzerland)* 20 (4). https://doi.org/10.3390/s20041173.
43. Abdalla, Aya, Christopher W. Atcherley, Pavithra Pathirathna, Srimal Samaranayake, Beidi Qiang, Edsel Peña, Stephen L. Morgan, Michael L. Heien, and Parastoo Hashemi. 2017. "*In Vivo Ambient Serotonin Measurements at Carbon-Fiber Microelectrodes.*" Analytical Chemistry 89 (18): 9703–11.
44. Castagnola, E., Vahidi, N. W., Nimbalkar, S., & Rudraraju, S. (2018). "*In Vivo Dopamine Detection and Single Unit Recordings Using Intracortical Glassy Carbon Microelectrode Arrays*." MRS Advances, 3(29), 1629–1634. https://doi.org/10.1557/adv.2018.98.
45. Castagnola, E, S Thongpang, M Hirabayashi, G Nava, S Nimbalkar, T Nguyen, S Lara, et al. 2021. "*Glassy Carbon Microelectrode Arrays Enable Voltage-Peak Separated Simultaneous Detection of Dopamine and Serotonin Using Fast Scan Cyclic Voltammetry*." Analyst 146 (12): 3955–70. https://doi.org/10.1039/d1an00425e.
46. Swamy, B. E., Kumara, B., and Venton, J., 2007. "*Carbon Nanotube-Modified Microelectrodes for Simultaneous Detection of Dopamine and Serotonin in Vivo*." *Analyst* 132 (9): 876–84. https://doi.org/10.1039/b705552h.
47. Qin, Si, Miranda Van Der Zeyden, Weite H. Oldenziel, Thomas I.F.H. Cremers, and Ben H.C. Westerink. 2008. "*Microsensors for in Vivo Measurement of Glutamate in Brain Tissue," Sensors* 8 (11): 6860–84. https://doi.org/10.3390/s8116860.

48. Van der Zeyden, M., Oldenziel, W. H., Rea, K., Cremers, T. I., & Westerink, B. H. (2008). *Microdialysis of GABA and Glutamate: Analysis, Interpretation and Comparison with Microsensors,"* Pharmacology Biochemistry and Behavior, 90(2), 135–147. https://doi.org/10.1016/j.pbb.2007.09.004
49. Meng, L., Wu, P., Chen, G., Cai, C., Sun, Y., & Yuan, Z. (2009). "*Low Potential Detection of Glutamate Based on the Electrocatalytic Oxidation of NADH at Thionine/Single-Walled Carbon Nanotubes Composite Modified Electrode,"* Biosensors and Bioelectronics, 24(6), 1751–1756.
50. Vomero, Maria, Elisa Castagnola, Francesca Ciarpella, Emma Maggiolini, Noah Goshi, Elena Zucchini, Stefano Carli, Luciano Fadiga, Sam Kassegne, and Davide Ricci. 2017. "*Highly Stable Glassy Carbon Interfaces for Long-Term Neural Stimulation and Low-Noise Recording of Brain Activity*." *Scientific Reports* 7 (December 2016): 1–14. https://doi.org/10.1038/srep40332.
51. Vomero, M., Van Niekerk, P., Nguyen, V., Gong, N., Hirabayashi, M., Cinopri, A., Logan, K., Moghadasi, A., Varma, P., and Kassegne. S., 2016. "*A Novel Pattern Transfer Technique for Mounting Glassy Carbon Microelectrodes on Polymeric Flexible Substrates*." Journal of Micromechanics and Microengineering 26 (2). doi.org/10.1088/0960-1317/26/2/025018.
52. Nimbalkar, S., Castagnola, E., Balasubramani, A., Scarpellini, A., Samejima, S., Khorasani, A., Boissenin, A., Thongpang, S., Moritz, C., and Kassegne, S., "*Ultra-Capacitive Carbon Neural Probe Allows Simultaneous Long-Term Electrical Stimulations and High-Resolution Neurotransmitter Detection"*, Nature Scientific Reports 8 (1), 6958, 2018**.**
53. Bisgaard SI, Nguyen LQ, Bøgh KL, Keller SS. "*Dermal Tissue Penetration of In-plane Silicon Microneedles Evaluated in Skin-Simulating Hydrogel, Rat Skin and Porcine Skin*" Biomater Adv. Dec 2023, DOI: 10.1016/j.bioadv.2023.213659. Epub 2023 Oct 10. PMID: 37939443.
54. Pomfret, Roland, Gurwattan Miranpuri, and Karl Sillay. 2013. "*The Substitute Brain and the Potential of the Gel Model*." Annals of Neurosciences 20 (3): 118–22.
55. Budday, Silvia, Timothy C. Ovaert, Gerhard A. Holzapfel, Paul Steinmann, and Ellen Kuhl. 2020. "*Fifty Shades of Brain: A Review on the Mechanical Testing and Modeling of Brain Tissue*," Archives of Computational Methods in Engineering. Vol. 27. Springer Netherlands.
56. Singh, D., S. Boakye-Yiadom, and D. S. Cronin. 2019. "*Comparison of Porcine Brain Mechanical Properties to Potential Tissue Simulant Materials in Quasi-Static and Sinusoidal Compression*." Journal of Biomechanics 92: 84–91. https://doi.org/10.1016/j.jbiomech.2019.05.033.
57. van Duin, A.C.T., Dasgupta, S., Lorant, F., Goddard, W.A., *"ReaxFF: A Reactive Force Field for Hydrocarbons*", J. Phys. Chem. A, 105, 9396-9409, 2001.
58. Montgomery-Walsh, R., Nimbalkar, S., Bunnell, J., Galindo, S., Kassegne, S., "*Molecular Dynamics Simulation of Evolution of Nanostructures and Functional Groups in Glassy Carbon Under Pyrolysis"*, Carbon 184 (2021) 627 – 640
59. Senftle, T., Hong, S., Islam, M. *et al*. "*The ReaxFF Reactive Force-Field: Development, Applications and Future Directions*", NPI Comput Mater 2, 15011 (2016).
60. Russo, M. F. Jr and van Duin, A. C. T. "*Atomistic-Scale Simulations of Chemical Reactions: Bridging from Quantum Chemistry to Engineering*," Nucl. Instrum. Methods Phys. Res. B 269, 1549–1554 (2011).
61. Nandiyanto, A, R Oktiani, and R Ragadhita. 2019. "*How to Read and Interpret FTIR Spectroscope of Organic Material*." Indonesian Journal of Science and Technology 4 (1): 97–118. https://doi.org/10.17509/ijost.v4i1.15806.
62. Mureşan-Pop, M, I Kacsó, X Filip, E Vanea, G. Borodi, N. Leopold, I. Bratu, and S. Simon. 2011. "*Spectroscopic and Physical-Chemical Characterization of Ambazone-Glutamate Salt*." Spectroscopy 26 (2): 115–28. https://doi.org/10.3233/SPE-2011-0519.
63. Jayaraman, V.;Keesey, R.; Madden, D. R., *"Ligand–Protein Interactions in the Glutamate Receptor,"* Biochemistry **2000**, 39, 8693– 8697, https://doi.org/10.1021/bi000892f
64. Batra, B., & Pundir, C. S. (2013). "*An Amperometric Glutamate Biosensor Based on Immobilization of Glutamate Oxidase onto Carboxylated Multiwalled Carbon Nanotubes/Gold Nanoparticles/Chitosan Composite Film Modified Au Electrode*," Biosensors and Bioelectronics, 47, 496–501. https://doi.org/10.1016/j.bios.2013.03.063
65. Tonel, M.Z, M González-Durruthy, I Zanella, and S.B Fagan. 2019. "*Interactions of Graphene Derivatives with Glutamate-Neurotransmitter: A Parallel First Principles - Docking Investigation*." Journal of Molecular Graphics and Modelling 88: 121–27.
66. Sanford AL, Morton SW, Whitehouse KL, Oara HM, Lugo-Morales LZ, Roberts JG, Sombers LA. Voltammetric detection of hydrogen peroxide at carbon fiber microelectrodes. Anal Chem. 2010 Jun 15;82(12):5205-10